SEMARAK ILMU PUBLISHING

Journal of Advanced Research in Fluid Mechanics and Thermal Sciences

Journal homepage:
https://semarakilmu.com.my/journals/index.php/fluid_mechanics_thermal_sciences/index
ISSN: 2289-7879

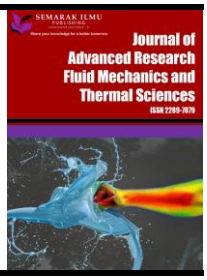


# The Effect of Viscous Dissipation and Chemical Reaction on the Flow of MHD Nanofluid

Batcha Srisailam[1], Katkoori Sreeram Reddy[2], Ganji Narender[3,*], Bala Siddhulu Malga[4]

[1] Department of Humanities & Sciences (Mathematics), Government Polytechnic, Tirumalgiri, Suryapet, Telangana, India
[2] Department of Mathematics, Osmania University, Hyderabad, Telangana, India
[3] Department of Humanities & Sciences (Mathematics), CVR College of Engineering, Hyderabad, Telangana, India
[4] Department of Mathematics, GITAM University, Hyderabad Campus, Telangana, India

**ARTICLE INFO**

***Article history:***
Received 2 April 2023
Received in revised form 16 June 2023
Accepted 22 June 2023
Available online 10 July 2023

***Keywords:***
Magnetic effect; nanofluid; viscous dissipation; chemical reaction; thermophoresis; Brownian motion

**ABSTRACT**

A numerical investigation is performed for the MHD viscous nanofluid due to convective stretching. Heat and mass transfer are investigated for steady, viscous dissipations and chemical reactions. The governing partial differential equations are transformed into an arrangement of the non-linear ordinary differential equations by using the similarity transformation. Utilising the shooting method, the system of ordinary differential equations has been solved with the help of the computational language FORTRAN to compute the numerical results. The numerical solution obtained for the velocity, temperature, and concentration profiles has been presented through graphs for different choices of physical parameters. The numerical values of the Nusselt and Sherwood numbers have also been presented and analysed through tables.

## 1. Introduction

The study of fluid on a stretched surface is one of the most significant topics explored in the modern period since it happens in many technical processes such as extrusion, wire drawing, melt whirling, glass fibre manufacture, rubber sheet production, and the cooling of massive metallic plates such as an electrolyte. Crane [1] discovered the incompressible flow by applying a consistent load to a sheet. This problem drew the attention of other mathematicians, who solved it further by considering various physical circumstances [2–5]. Makinde [6] investigated the flow of nanofluids through a flat plate's boundary layer. They went on to investigate the effects of viscous dissipation and Newtonian heating on various geometry types, including porous surfaces.

Convective heat transfer refers to the flow of fluids from one location to another to transfer heat. Convective heat transfer is the combination of heat diffusion and bulk fluid flow, also known as conduction and advection. Convective heat transfer has several uses in engineering. A large number of studies on nanofluids (fluid-nanoparticle mixtures) suggest that they can enhance thermal

* *Corresponding author.*
*E-mail address: gnriimc@gmail.com*

https://doi.org/10.37934/arfmts.107.2.150170

conductivity in fluids. The term "nanofluid" refers to a fluid that contains nanometer-sized particles known as nanoparticles. Many researchers use MHD flow because of its wide variety of applications. Ibrahim *et al.,* [7] investigated the impact of time dependent MHD on viscous dissipation and radiation. Zhang *et al.,* [8] quantitatively investigated the impact of radiation, heat flux, and chemical reactions on the heat transfer of nanofluids across porous media. They also looked into how magnetohydrodynamics affected the thermal boundary layer of a viscous fluid.

Viscous dissipations in heat transmission indicate that the fluid gets heated from multiple sources. In this mechanism, the viscosity of the fluid absorbs heat from kinetic energy and converts it to internal energy for the system. Alam *et al.,* [9] investigated Joule heating and viscous dissipation on an inclined isothermal permeable surface using MHD and thermophoresis. Hayat *et al.,* [10] investigated the incompressible, unsteady, three-dimensional MHD flow over a stretched sheet with viscous dissipation and Joule heating. Viscous dissipation is vital for natural convection in a variety of systems.

Afify [11] investigated the MHD-free convective heat and fluid flow passing across the stretched surface while performing a chemical reaction. Zhang *et al.,* [12] quantitatively investigated the effects of radiation, heat flux, and chemical reactions on nanofluid heat transfer across porous media. Poornima *et al.,* [13] investigate the effects of viscous dissipation and Joule heating on thermal boundary layer flow. Anwar *et al.,* [14] investigated the combined effects of heat and mass transmission of nanofluids over a nonlinear stretching sheet.

In a study conducted by Nadia Diana Rusdi *et al.,* [15], the focus was on investigating the effects of the nanoparticle volume fraction parameter and temperature-dependent viscosity on various thermal and flow characteristics. Daniel John Ebrahim Bryant, and K. C. Ng.[16] examined the Volume of Fluid (VOF) approach used to track the air-water interface. Mani Ramanuja *et al.,* [17] explored the heat exchange of the flow within the nanofluid flow problem in the present first-order chemical reaction. Rahimah Mahat *et al.,* [18] explored a mathematical model for free convection boundary flow on a horizontal circular cylinder in a viscoelastic nanofluid has been constructed in this paper with boundary conditions constant heat flux.

Patil Priyanka *et al.,* [19], examined the two-dimensional Casson nano liquid motion predicaments, adjacent to the boundary level over the stretching sheet via non-Darcian porous medium. Jagadish *et al.,* [20] addressed the issue of the steady laminar 2D flow along with nanofluid sheet transfer from Casson through a permeable linearly stretching sheet. Gul *et al.,* [21] examined the optimal homotopy analysis (OHAM) technique has been examined to solve the laminar magnetohydrodynamic flow (MHD flow) on the upper-convected Maxwell fluid on an isothermal porous stretch surface. Subhas Abel *et al.,* [22] studied the impact of the magnetohydrodynamic boundary layer flow and heat transfer characteristics of a laminar liquid film over a flat impermeable stretching sheet in the presence of a non-uniform heat source/sink. Subhas Abel *et al.,* [23] the effect of MHD flow and heat transfer within a boundary layer flow on an upper-convected Maxwell (UCM) fluid over a stretching sheet is examined.

Mahnoor Sarfraz *et al.,* [24] analyzed Homann stagnation point flow with nanoparticles scattered in water over a porous spiraling disk. Masood Khan, Mahnoor Sarfraz, and Awais Ahmed [25] studied the Jeffrey's nanofluid for a modification of Homann's exterior potential flow in the stagnation region is modeled over a cylindrical disk. M. Khan *et al.,* [26] examined the heat transfer of Homann flow in the stagnation region of the $Al_2O_3$-Cu/water hybrid nanofluid is investigated by adopting the Tiwari-Das model over a cylindrical disk. Mahnoor and Masood Khan [27] studied the electromagnetically conducting flow consisting of carbon nanotubes suspension immersed with ethylene glycol is scrutinized on a surface which is stretching biaxially, planarly, and perpendicularly.

Narender *et al.,* [28] studied the impact of the radiation effects in the presence of heat generation/absorption and magnetic field on the magnetohydrodynamics (MHD) stagnation point flow over a radially stretching sheet using a Casson nanofluid. Narender *et al.,* [29] examined the viscous dissipation and thermal radiation effects on the MHD mixed convection stagnation point flow of Maxwell nanofluid over a stretching surface. Narender *et al.,* [30] explored the impacts of external magnetic field inclinations and viscous dissipation due to heat generation or absorption parameter on MHD mixed convective flow of Casson nanofluid.

In this paper, an extension of the model presented by D. Makinde *et al.,* [31] is presented, focusing on the inclusion of chemical reaction and viscous dissipation effects. The Adams Moulton method is employed to solve the similarity equations derived from the governing boundary layer equations, utilizing similarity transformations.

The structure of the paper is organized as follows: Section 3 introduces the problem formulation and outlines the quantities of physical interest that will be investigated. Section 4 presents the application of the Adams Moulton method to solve the proposed problem, detailing the computational approach. Section 5 focuses on the validation of the Adams Moulton method solution through code validation techniques, ensuring the accuracy and reliability of the numerical approach. Section 6 presents the results obtained from the analysis and subsequent discussions. The findings and their implications are discussed in detail. Finally, Section 7 provides concluding remarks summarizing the key outcomes of the study and potentially suggesting avenues for further research.

## 2. Formulation of the Problem

Consider a steady flow of an incompressible electrically conducting and radiating nanofluid in the region $y>0$ induced by a permeable stretching surface located at $y=0$ with a fixed origin at $x=0$ as displayed in Figure 1. From the slot at the origin thin solid surface is extruded which is being stretched in $x-$ direction. The stretching velocity $u_w(x)=U_0x^m$, where $U_0$ is the uniform velocity and $m>0$ is a constant parameter. Along $y-$ axis, a constant magnetic field of strength $B_0$ is applied perpendicular to x-axis.

The flow is described by the equation of continuity, equation of momentum and the energy equation as:

$$\frac{\partial u}{\partial x}+\frac{\partial v}{\partial y}=0, \tag{1}$$

$$\begin{aligned}\frac{\partial p}{\partial x}=&-\rho_f\left(u\frac{\partial u}{\partial x}+v\frac{\partial u}{\partial y}\right)+\mu\frac{\partial^2 u}{\partial y^2}+\left(1+C_\infty\right)\rho_{f\infty}\beta_T g\left[T-T_\infty\right]\\&-\left(\rho_p-\rho_{f\infty}\right)\beta_C g\left[C-C_\infty\right]-\sigma B_0^2 u,\end{aligned} \tag{2}$$

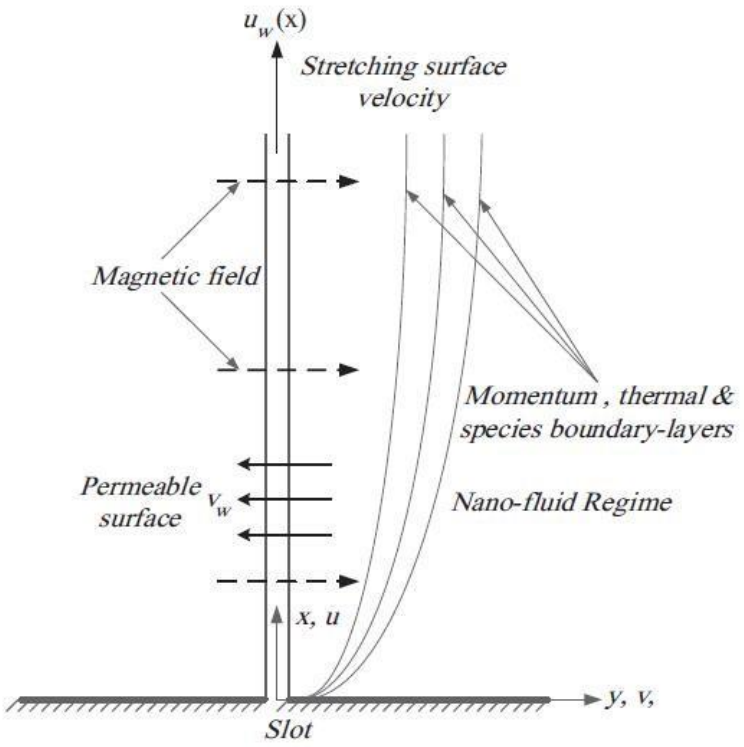


**Fig. 1.** Geometry for the flow

$$u\frac{\partial T}{\partial x}+v\frac{\partial T}{\partial y}=\alpha\left(\frac{\partial^2 T}{\partial y^2}\right)-\frac{1}{(\rho c)_f}\frac{\partial q_r}{\partial y}-\frac{Q'}{(\rho c)_f}(T-T_\infty)+\tau\left[D_B\frac{\partial C}{\partial y}\frac{\partial T}{\partial y}+\frac{D_T}{T_\infty}\left(\frac{\partial T}{\partial y}\right)^2\right]+\frac{\nu}{(\rho c)_f}\left(\frac{\partial u}{\partial y}\right)^2 \tag{3}$$

$$u\frac{\partial C}{\partial x}+v\frac{\partial C}{\partial y}=D_B\left(\frac{\partial^2 C}{\partial y^2}\right)+\frac{D_T}{T_\infty}\left(\frac{\partial^2 T}{\partial y^2}\right)-k_0(C-C_\infty), \tag{4}$$

The associated BCs:

$$\left.\begin{aligned}&u=U_w(x)=U_0x^m,\quad v=0,\quad T=T_w,\quad C=C_w\quad at\ \ y=0,\\&u\to 0,\quad v\to 0,\quad T\to T_\infty,\quad C\to C_\infty\quad as\quad y\to\infty.\end{aligned}\right\} \tag{5}$$

In Eq. (1) to Eq. (4), $u$ and $v$ denote the components of fluid velocity along $x$ and $y$ direction, respectively, $\rho_f$ the nanofluid density, $\rho$ the density of the nanoparticle, $\beta_T$ the coefficient of volumetric thermal expansion, $\beta_C$ the coefficient of volumetric concentration expansion, $g$ the acceleration due to gravity, $B_0$ the magnetic induction, $\alpha$ the thermal diffusivity of the nanofluid, $\nu$ the kinematic viscosity, $D_B$ the coefficient of Brownian diffusion, $D_T$ the coefficient of thermophoresis diffusion, $(\rho c)_f$ the heat capacity of the fluid and $(\rho c)_p$ denotes the heat capacity of

the nanoparticle, $q_r$ radiative heat flux, $\kappa$ the thermal conductivity, $\tau = \frac{(\rho c)_p}{(\rho c)_f}$ is the ratio of nanoparticle heat capacity and the base fluid heat capacity. In the modelled problem, $T$ denotes the temperature of the nanofluid, $C$ the concentration of the nanofluid, $T_w, and\ C_w$ the temperature and concentration along the stretching sheet $T_w$, $T_\infty$ and $C_\infty$ the ambient temperature and concentration, respectively, $Q^{'}$ is the coefficient of heat generation parameter and $k_0$ is the rate of chemical reaction parameter.

## 3. Dimensionless Form of the Governing Equations

In this section, we translate the system of Eq. (1) to Eq. (4), as well as the boundary conditions Eq. (5), into a dimensionless form. We utilize the similarity transformation to determine our model's answer.

$$\eta = \sqrt{\frac{(m+1)U_0 x^{m-1}}{2\,\nu}},\ \psi = \sqrt{\frac{2\nu U_0\, x^{m-1}}{(m+1)}}\, f(\eta),\ \theta(\eta) = \frac{T - T_\infty}{T_w - T_\infty}, \phi(\eta) = \frac{C - C_\infty}{C_w - C_\infty}. \tag{6}$$

In above, $\psi(x, y)$ denotes stream function obeying.

$$u = \frac{\partial \psi}{\partial y},\ \ v = -\frac{\partial \psi}{\partial x} \tag{7}$$

The continuity Eq. (1) is satisfied identically, and the impact of the stream function on the remaining three equations, momentum Eq. (2), temperature Eq. (3), and concentration Eq. (4), is as follows:

$$f''' + ff'' - \frac{2m}{m+1}\left(f'\right)^2 + \frac{2}{m+1}(\lambda\theta - \delta\phi) - Mf' = 0, \tag{8}$$

$$\frac{(1+R)}{\Pr}\theta'' + f\theta' + Nb\phi'\theta' + Nt\left(\theta^1\right)^2 + Ec\left(f''\right)^2 + Q'\theta = 0, \tag{9}$$

$$\phi'' + Le\, f\phi' + \frac{Nt}{Nb}\theta'' - \gamma\, Le\,\phi = 0. \tag{10}$$

The BCs get the form:

$$\left.\begin{aligned} &At\ \ \eta = 0,\ f(\eta) = 0,\ f'(\eta) = 1,\ \theta(\eta) = 1,\ \phi(\eta) = 1 \\ &At\ \ \eta \to \infty,\ \ 0\, f'(\infty) \to 0, \theta(\infty) \to 0, \phi(\infty) \to 0. \end{aligned}\right\} \tag{11}$$

In Eq. (8) to Eq. (10), the governing parameters are defined as

$Gr = \dfrac{(1-C_\infty)\rho_{f\infty} gn(T_w - T_\infty)}{\rho_f \nu^2 \mathrm{Re}_x^{1/2}}$, is the local thermal Grashof number, $Gr = \dfrac{(\rho_f - \rho_{f\infty}) gn_1 (C_w - C_\infty)}{\rho_f \nu^2 \mathrm{Re}_x^{1/2}}$, is the local concentration Grashof number, $\lambda = \dfrac{Gr}{\mathrm{Re}_x^{1/2}}$ is the buoyancy parameter, $\lambda = \dfrac{Gm}{\mathrm{Re}_x^{1/2}}$ is the solutal buoyancy parameter, $\nu = \dfrac{\mu}{\rho_f}$ is the kinematic viscosity of the nanofluid, $P\mathrm{r} = \dfrac{\nu}{\alpha}$, is Prandtl number, $Le = \dfrac{\nu}{D_\mathrm{B}}$, is Lewis number, $Nb = \dfrac{(\rho c)_p D_\mathrm{B} (C_w - C_\infty)}{\nu (\rho c)_f}$, is Brownian motion parameter, $Nt = \dfrac{(\rho c)_p D_T (T_e - T_\infty)}{\nu (\rho c)_f T_\infty}$, is thermophoresis parameter and $Ec = \dfrac{u_w^2}{(\rho c)_f (T_w - T_\infty)}$, is the Eckert number and $\gamma = \dfrac{k_0}{a}$, is the chemical reaction parameter.

In this problem, the desired physical quantities are the local Nusselt number $Nu_x$, and reduced Sherwood number $Sh_x$ and the skin-friction coefficient $C_{fx}$. These quantities are defined as

$$C_{fx} = \frac{\tau_w}{\rho u_w^2},\ Nu_x = \frac{x q_w}{k(T_w - T_\infty)},\ Sh_x = \frac{x q_m}{D_B (C_w - C_\infty)} \tag{12}$$

In the above equations $q_w$ represents the heat flux, $\tau_w$ the shear stress, and $q_m$ denotes the mass flux which are defined as where the surface drag coefficient at the wall is given by

$$\tau_w = \mu\left(\frac{\partial u}{\partial y}\right)_{y=0},\ q_w = \left(-k\left(\frac{\partial T}{\partial y}\right)\right)_{y=0},\ q_m = -D_B\left(\frac{\partial C}{\partial y}\right)_{y=0}. \tag{13}$$

with the help of above equations, we get

$$C_{fx} = \frac{1}{\sqrt{2(m+1)}} \mathrm{Re}_x^{1/2} f''(0),\ Nu_x = -\sqrt{\frac{2}{(m+1)}} \mathrm{Re}_x^{1/2} \theta'(0),\ Sh_x = -\sqrt{\frac{2}{(m+1)}} \mathrm{Re}_x^{1/2} \phi'(0) \tag{14}$$

## 4. Solution Methodology

The analytic solution to the system of equations with matching boundary conditions Eq. (8) to Eq. (10) cannot be obtained since they are very nonlinear and coupled. So, we employ a numerical methodology, namely the shooting technique using the fourth-order Adam-Moulton method. To solve the system of ODEs Eq. (8) to Eq. (10) with boundary conditions Eq. (11) using the shooting technique, we must first transform these equation systems into a system of first-order differential equations.

For this purpose, let

$$\left.\begin{aligned} f = h_1,\ f' = h_2,\ f'' = h_3, \\ \theta = h_4,\ \theta' = h_5, \\ \phi = h_6,\ \phi' = h_7. \end{aligned}\right\} \tag{15}$$

The coupled nonlinear momentum, temperature, and concentration equations are then translated into a system of seven first-order differential equations, and the accompanying boundary conditions are changed into the form:

$$\left.\begin{aligned} h_1' &= h_2, \\ h_2' &= h_3, \\ h_3^1 &= \left[\frac{2m}{m+1}h_2^2 - h_1h_3 + M\,h_2 - \frac{2}{m+1}\left(\lambda h_4 - \delta h_6\right)\right], \\ h_4' &= h_5, \\ h_5^1 &= -\frac{\Pr}{(1+R)}\left[h_1h_5 + Nb\,h_5h_7 + Nt\,h_5^2 + Q'h_4 + Ec\,h_3^2)\right], \\ h_6' &= h_7, \\ h_7' &= \left[-Le\,h_1\,h_7 - \frac{Nt}{Nb}h_5' + Le\,\gamma\,h_6\right] \end{aligned}\right\} \tag{16}$$

$$\left.\begin{aligned} h_1(0) = 1,\ \ h_2(0) = 1,\ \ h_3(0) = r,\ \ h_4(0) = 1, \\ h_5(0) = s,\ \ \ \ h_6(0) = 1,\ \ h_7(0) = t. \end{aligned}\right\} \tag{17}$$

The aforementioned equations (20) are solved with an initial guess $r^{(0)}$, $s^{(0)}$, $t^{(0)}$ using the Adam-Moulton technique of order 4. The Newton's method approach is used to update these estimations. The iterative method is performed until the following conditions are fulfilled, $\max\left(\left|y_2(\eta_\infty)\right|, \left|y_4(\eta_\infty)\right| \left|y_6(\eta_\infty)\right|\right) < \in$, where $\in > 0$ tolerance is defined: We have fixed $\in = 10^{-5}$. all computations in this paper. The selection $\eta_{\max} = 8$ was more than enough for the ultimate condition. The convergence requirement is set to agree on successive values up to three significant digits.

## 5. Code Validation

Table 1 compares the current results with some of the earlier published work on free convection [13,14,30] in order to validate the code used for the numerical solution of equations governing natural convective flow. Results obtained from the current code are in good agreement with the published results [13,14,30].

**Table 1**
Comparison of current code results with some earlier results of [13,14,30], when $m=1,\ \Pr = Le = 10,$ $\lambda = \gamma = M = N = Q = Ec = 0.$

| Parameters | | Anwar *et al.,* [14] | | Poornima and Reddy [13] | | Makinde [30] | | Present results | |
|---|---|---|---|---|---|---|---|---|---|
| $Nb$ | $Nt$ | $-\theta'(0)$ | $-\phi'(0)$ | $-\theta'(0)$ | $-\phi'(0)$ | $-\theta'(0)$ | $-\phi'(0)$ | $-\theta'(0)$ | $-\phi'(0)$ |
| 0.1 | 0.1 | 0.9524 | 2.1294 | 0.952376 | 2.12939 | 0.952376 | 2.129388 | 0.9523372 | 2.1290970 |
| 0.2 | 0.2 | 0.3654 | 2.5152 | 0.365357 | 2.51522 | 0.365358 | 2.515217 | 0.3653571 | 2.5148870 |
| 0.3 | 0.3 | 0.1355 | 2.6088 | 0.135514 | 2.60881 | 0.135514 | 2.608812 | 0.1355215 | 2.6084690 |
| 0.4 | 0.4 | 0.0495 | 2.6038 | 0.049465 | 2.60384 | 0.049464 | 2.603839 | 0.0494710 | 2.6034900 |
| 0.5 | 0.5 | 0.0179 | 2.5731 | 0.017922 | 2.5731 | 0.017922 | 2.573099 | 0.0179259 | 2.5727470 |

Table 2 shows the effect of different physical parameters, for example, the magnetic parameter, stretching parameter, solutal buoyancy parameter, thermophoresis parameter, Brownian motion parameter, Eckert number, and chemical reaction parameter, and their impact on the skin-friction coefficient, Nusselt number, and Sherwood number. From this table, it is noted that an increase in the magnetic parameter, stretching parameter, solutal buoyancy parameter, and thermophoresis parameter enhances the local skin-friction coefficient. Furthermore, the skin friction coefficient decreases by enlarging the values of the Brownian motion parameter, chemical reaction parameter, Lewis number, viscous dissipation, heat generation parameter, buoyancy parameter, radiation parameter, and Prandtl number.

**Table 2**
Computations of the skin friction coefficient $-f''(0)$, Nusselt number $-\theta'(0)$ and the Sherwood number $-\phi'(0)$ for various values of $Nb, Nt, \Pr, Le, \lambda, \delta, m, R, M, Q, Ec, \gamma.$

| $Nb$ | $Nt$ | $Pr$ | $Le$ | $\lambda$ | $\delta$ | $m$ | $R$ | $M$ | $Q$ | $Ec$ | $\gamma$ | $-f''(0)$ | $-\theta'(0)$ | $-\phi'(0)$ |
|---|---|---|---|---|---|---|---|---|---|---|---|---|---|---|
| 0.1 | 0.1 | 0.71 | 10 | 1 | 1 | 1 | 0.2 | 0.5 | 0.1 | 0.2 | 0.2 | 0.8346336 | 0.3333888 | 2.7127630 |
| 0.5 | 0.1 | 0.71 | 10 | 1 | 1 | 1 | 0.2 | 0.5 | 0.1 | 0.2 | 0.2 | 0.8188873 | 0.2683586 | 2.7372840 |
| 0.1 | 0.3 | 0.71 | 10 | 1 | 1 | 1 | 0.2 | 0.5 | 0.1 | 0.2 | 0.2 | 0.9007490 | 0.2387225 | 1.1291710 |
| 0.1 | 0.1 | 5.0 | 10 | 1 | 1 | 1 | 0.2 | 0.5 | 0.1 | 0.2 | 0.2 | 1.0645800 | 0.4929985 | 2.7770070 |
| 0.1 | 0.1 | 0.71 | 25 | 1 | 1 | 1 | 0.2 | 0.5 | 0.1 | 0.2 | 0.2 | 0.7702647 | 0.3387359 | 4.3936610 |
| 0.1 | 0.1 | 0.71 | 10 | 2 | 1 | 1 | 0.2 | 0.5 | 0.1 | 0.2 | 0.2 | 0.3401598 | 0.4037667 | 2.7670530 |
| 0.1 | 0.1 | 0.71 | 10 | 1 | 2 | 1 | 0.2 | 0.5 | 0.1 | 0.2 | 0.2 | 1.0359080 | 0.3215477 | 2.6973040 |
| 0.1 | 0.1 | 0.71 | 10 | 1 | 1 | 5 | 0.2 | 0.5 | 0.1 | 0.2 | 0.2 | 1.2560580 | 0.2284546 | 2.6710150 |
| 0.1 | 0.1 | 0.71 | 10 | 1 | 1 | 1 | 1.0 | 0.5 | 0.1 | 0.2 | 0.2 | 0.7791331 | 0.2678639 | 2.7286410 |
| 0.1 | 0.1 | 0.71 | 10 | 1 | 1 | 1 | 0.2 | 1.0 | 0.1 | 0.2 | 0.2 | 1.2259210 | 0.1654789 | 1.1354960 |
| 0.1 | 0.1 | 0.71 | 10 | 1 | 1 | 1 | 0.2 | 0.5 | 0.15 | 0.2 | 0.2 | 0.8215425 | 0.2997889 | 2.7291660 |
| 0.1 | 0.1 | 0.71 | 10 | 1 | 1 | 1 | 0.2 | 0.5 | 0.1 | 1.0 | 0.2 | 0.8074967 | 0.2206607 | 2.7811280 |
| 0.1 | 0.1 | 0.71 | 10 | 1 | 1 | 1 | 0.2 | 0.5 | 0.1 | 0.2 | 0.5 | 0.8107796 | 0.3060446 | 3.2317100 |

## 6. Results and Discussion

Makinde [31] used the HAM method for the numerical solution of the discussed model. In the present survey, the shooting technique along with Adams-Moulton Method of fourth order were opted for reproducing the solution of [31].

The effects of considered physical parameters have been calculated for $0.1 < Nt < 0.3,$ $0.1 < Nb < 0.3,\ 0 < M < 1.0,\ 0.2 \le R \le 3.0, 0 \le \lambda \le 1.0,\ 0 \le \delta \le 3.0,\ 0 \le m \le 5.0, 0.75 \le \Pr \le 5.0,$ $2.0 \le Le \le 15,$ for the further investigation of problem. The results have been depicted graphically and their detailed physical explanation is as follows:

### *6.1 Impact of Magnetic Parameter*

Figures 2 and 3 illustrate the influence of the magnetic parameter on the velocity profile and temperature distribution. The figures demonstrate that the thickness of the velocity boundary layer reduces as the magnetic parameter increases, although the temperature distribution increases somewhat as the magnetic parameter increases. It is caused by the Lorentz force, which is produced when a magnetic field is applied to a conducting fluid.

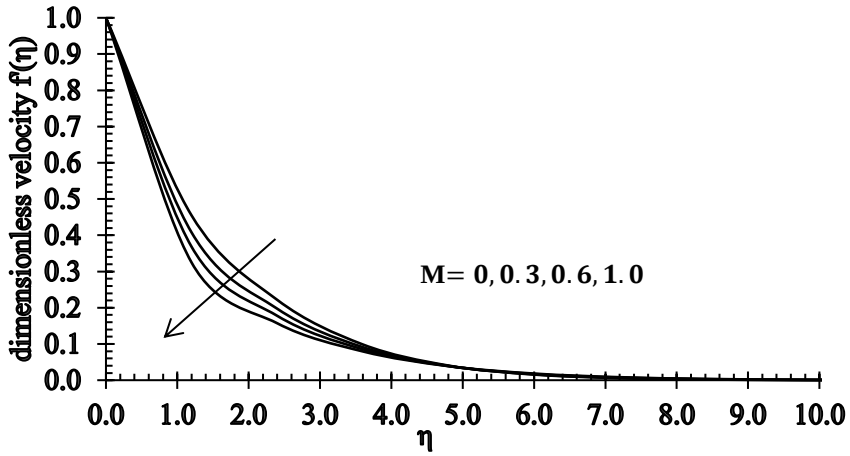


**Fig. 2.** The impact of $M$ on the velocity profile

Lorentz force has the propensity to lower flow speed, which validates our findings. When a magnetic field is applied to a fluid, the resistance of the fluid particles rises, resulting in an increase in temperature.

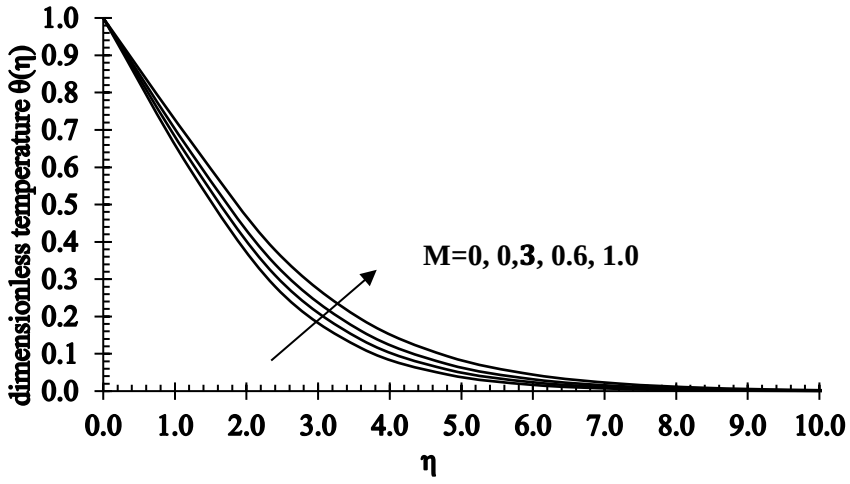


**Fig. 3.** The impact of $M$ on the temperature profile

### *6.2 Impact of the Buoyancy Parameter*

Figure 4 depicts the effect of thermal buoyancy parameter on the velocity. It is seen that as $\lambda$ increases, the velocity increases. This is due to the fact that the positive buoyancy force acts like a favorable pressure gradient and hence accelerates the fluid flow in the boundary layer. This results in higher velocity as $\lambda$ increases.

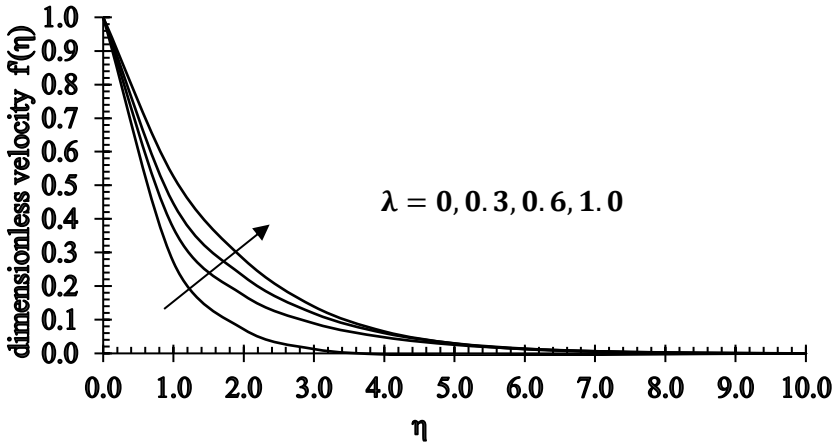


**Fig. 4.** The influence of $\lambda$ on the velocity profile

From the Figure 5, it is observed that the temperature along the surface decreases for the case of increasing buoyancy parameter but increases in the case of increase solutal buoyancy parameter.

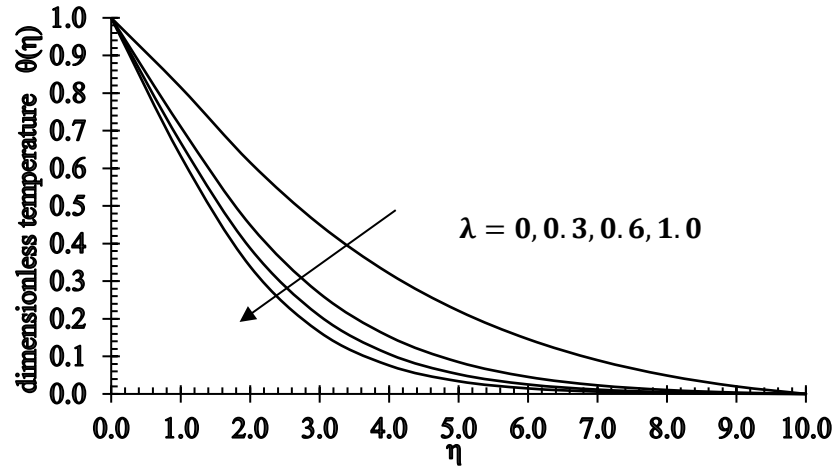


**Fig. 5.** Buoyancy parameter $\lambda$ for the temperature profile

*6.3 Impact of the Solutal Buoyancy Parameter*

The effect of the solutal buoyancy parameter on the velocity is displayed in Figure 6. It is seen that as the solutal buoyancy parameter increases, the velocity decreases.

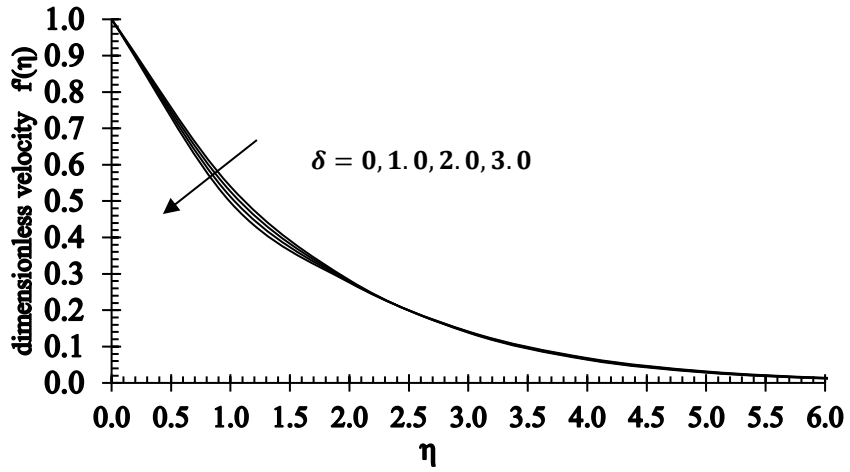


**Fig. 6.** The velocity profile on which $\delta$ has an effect

Figure 7 represents the impact of the solutal buoyancy parameter on temperature profile. The temperature rises with a rise in the solutal buoyancy parameter.

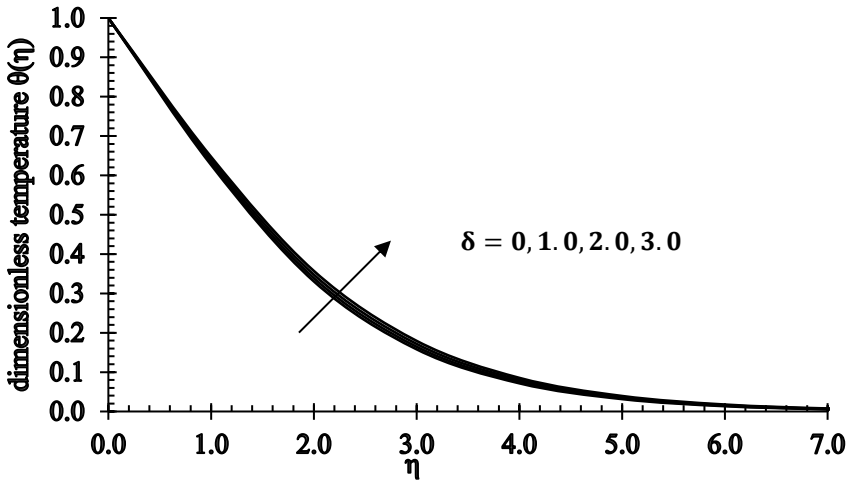


**Fig. 7.** The influence of $\delta$ on temperature profile

*6.4 Impact of the Stretching Parameter*

Figure 8 depicts the influence of the stretching parameter on velocity. As the stretching parameter is increased, the velocity falls.

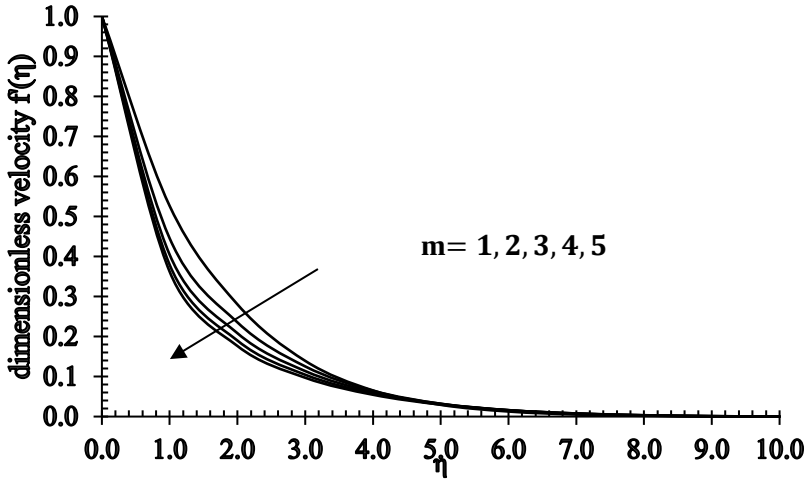


**Fig. 8.** Variation in velocity when of $m$ is varied

Figure 9 depicts the influence of the stretching parameter on temperature. It appears that the temperature rises as the stretching parameter increases.

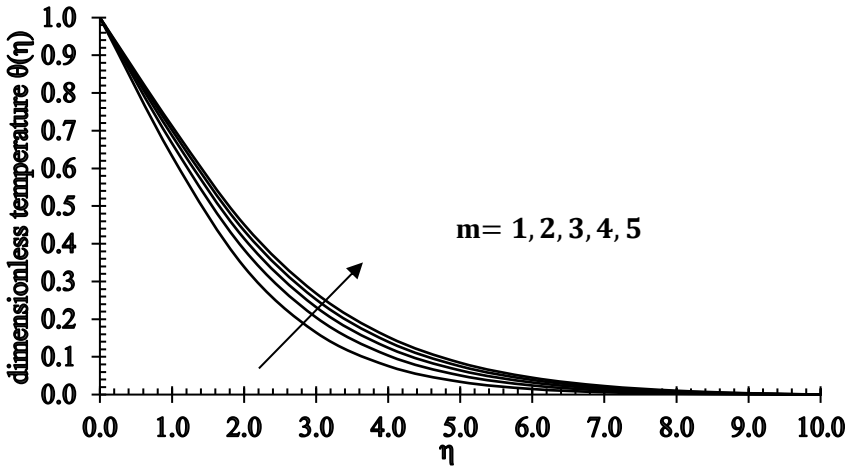


**Fig. 9.** Variation in temperature when $m$ is varied

*6.5 Impact of Prandtl Number*

Figure 10 depicts the impact of the Prandtl number on velocity. It has been discovered that increasing the Prandtl number causes the fluid to become more viscous, resulting in a drop in velocity.

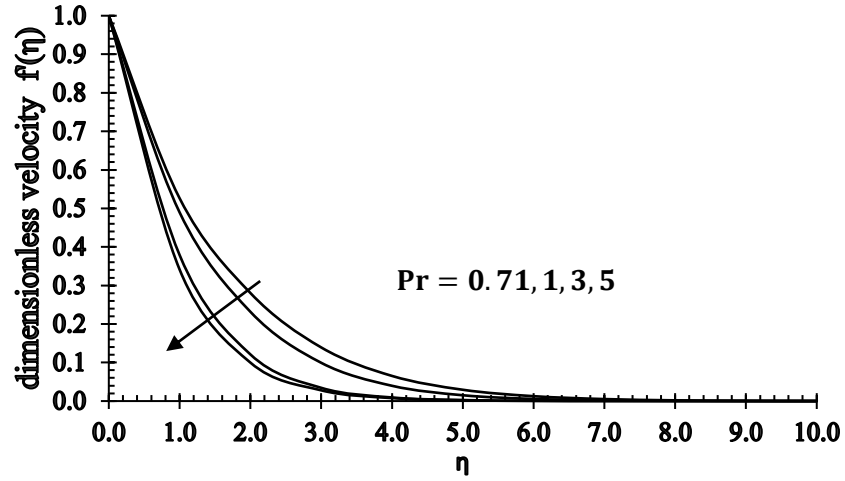


**Fig. 10.** Prandtl number $\mathrm{Pr}$ on the velocity profile

Figure 11 depicts the effect of the Prandtl number $\mathrm{Pr}$ on the temperature field profile. We can see from the graph that increasing the Prandtl number lowers the temperature profile. This is due to the fact that lower Prandtl numbers correspond to higher thermal conductivities, allowing heat to flow away from the stretched sheet. The temperature and thickness of the thermal boundary layer are reduced as a result of the change in thermal diffusivity.

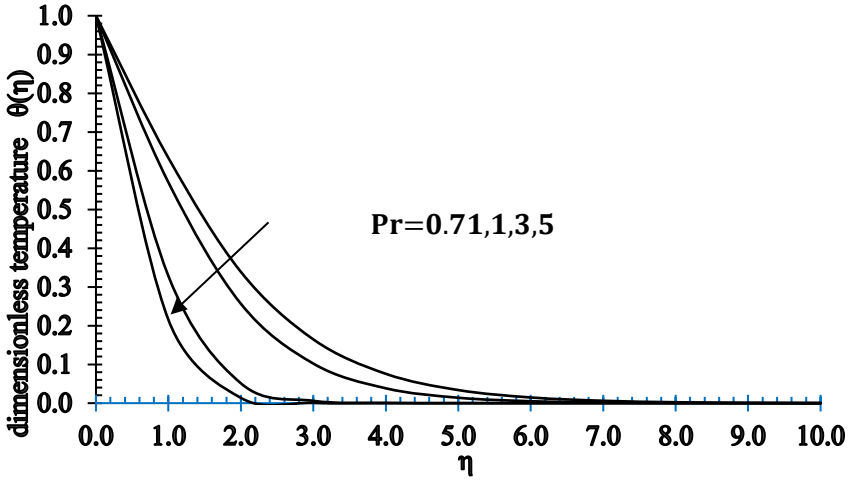


**Fig. 11.** Prandtl number $\mathrm{Pr}$ on the temperature profile

*6.6 Impact of Thermal Radiation Parameter*

Figures 12 and 13 depict the influence of thermal radiation on the velocity and temperature profiles, respectively. Figure 12 depicts the influence of the radiation parameter on velocity. The velocity rises as the radiation parameter increases.

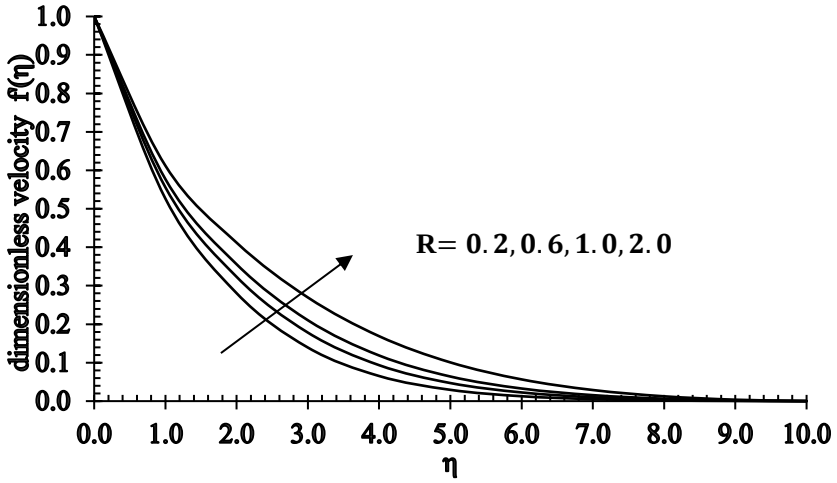


**Fig. 12.** Variation in Velocity when radiation parameter $R$ is varied

Figure 13 depicts temperature curves for various radiation parameter values. The temperature rises as the radiation parameter increases. The radiation parameter, which is the reciprocal of the stark number (also known as the Stephan number), quantifies the importance of thermal radiation transmission in comparison to heat conduction. Thus, bigger R values indicate a preference for heat radiation over conduction.

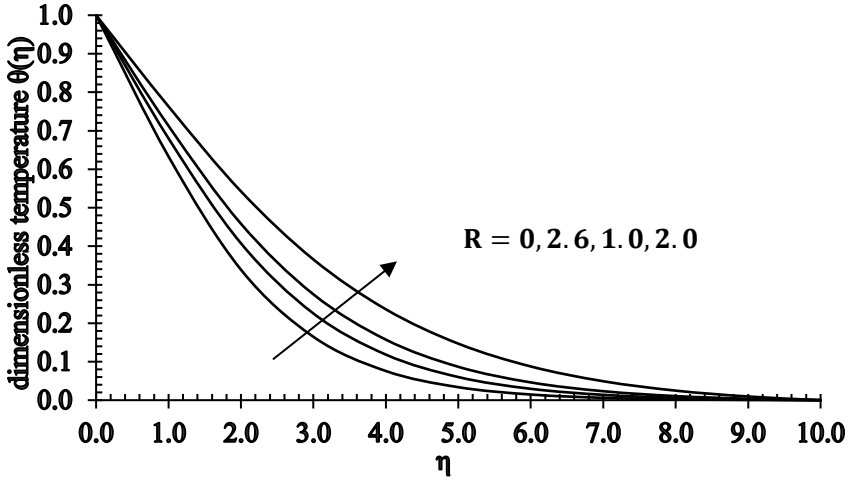


**Fig. 13.** Variation in Temperature when radiation parameter $R$ is varied

*6.7 Impact of Lewis Number on the Concentration*

The influence of the Lewis number on the concentration profile is seen in Figure 14. The ratio of thermal diffusion to molecular diffusion is known as the Lewis number. It is useful in determining the relationship between mass and heat transfer coefficient. The concentration profile becomes steeper as the Lewis number increases.

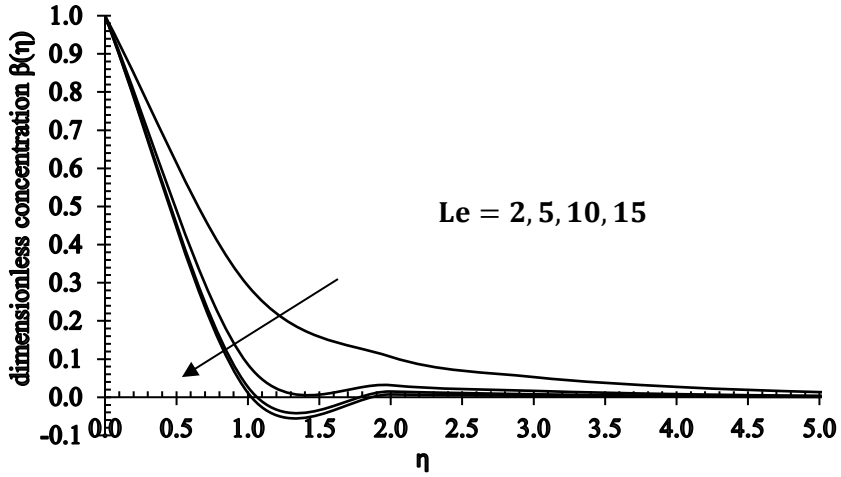


**Fig. 14.** The influence of Lewis number on concentration profile

*6.8 Impact of Heat Source Parameter*

Figure 15 demonstrates how increasing the heat source affects the velocity.

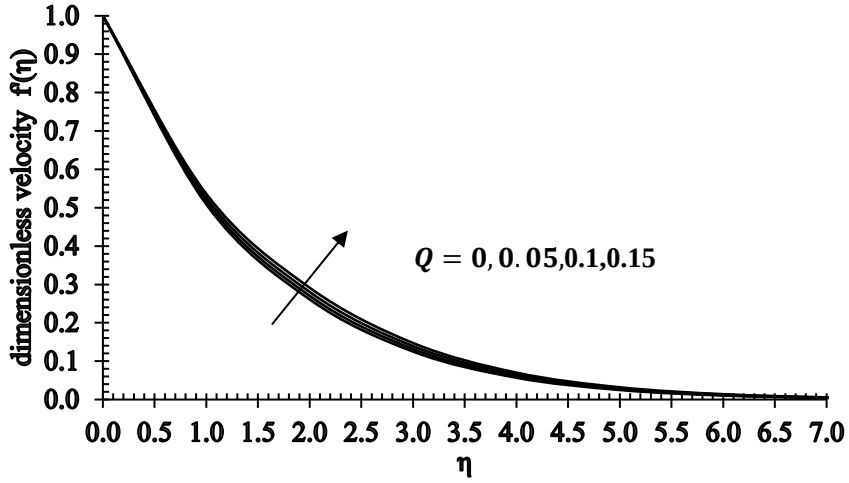


**Fig. 15.** Variation in velocity when $Q$ is varied

The temperature profiles for various values of heat source parameter are shown in Figure 16. It demonstrates that increasing the heat source improves the heat transport rate, resulting in a rise in temperature and the associated thermal boundary layer thickness $Q'$.

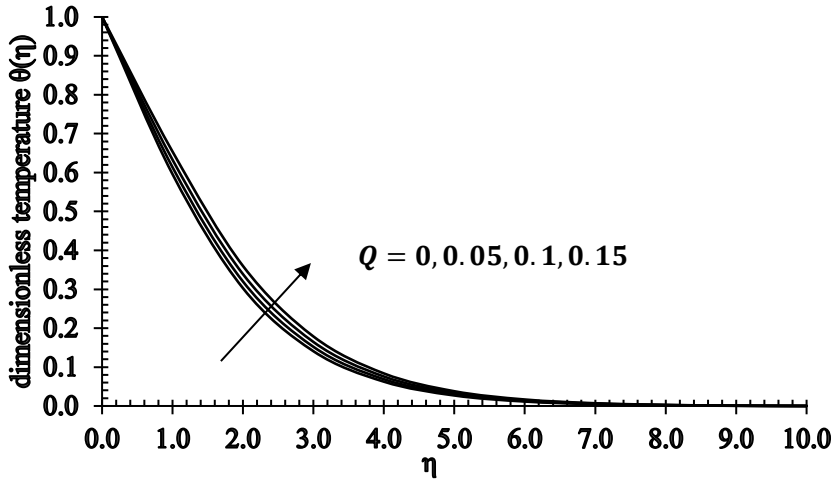


**Fig. 16.** Variation in temperature when $Q$ is varied

*6.9 The Impact of Viscous Dissipation*

Figure 17 shows the influence of $Ec$ on dimensionless temperature profile. Temperature profile increases with an increase in the values of Eckert number $Ec$. The Eckert number is defined as the ratio of kinetic energy wasted in the flow to thermal energy transmitted into or away from the fluid.

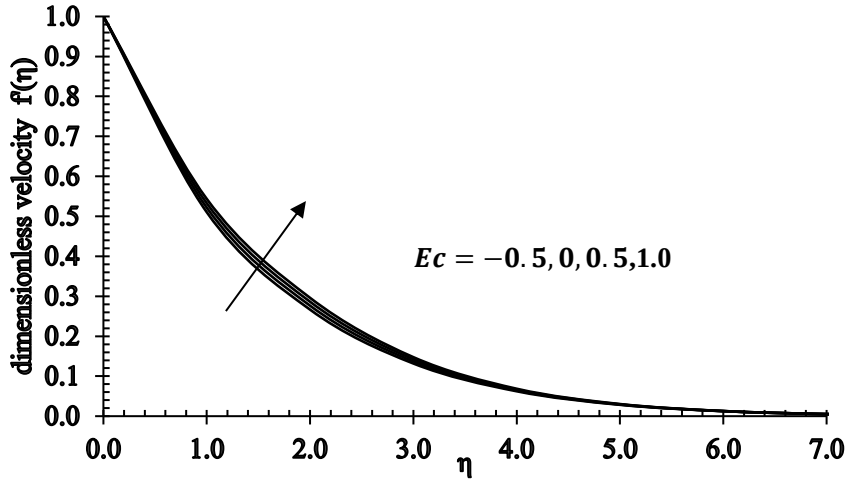


**Fig. 17.** Variation in velocity when $Ec$ is varied

This graph indicates that when the Eckert number for the temperature profile grows, so does the temperature distribution profile. We may conclude that the presence of viscous dissipation increases the tangential velocity $f'$ (Figure 18) and the temperature $\theta$. This rise in the temperature is due to the heat created by viscous dissipation.

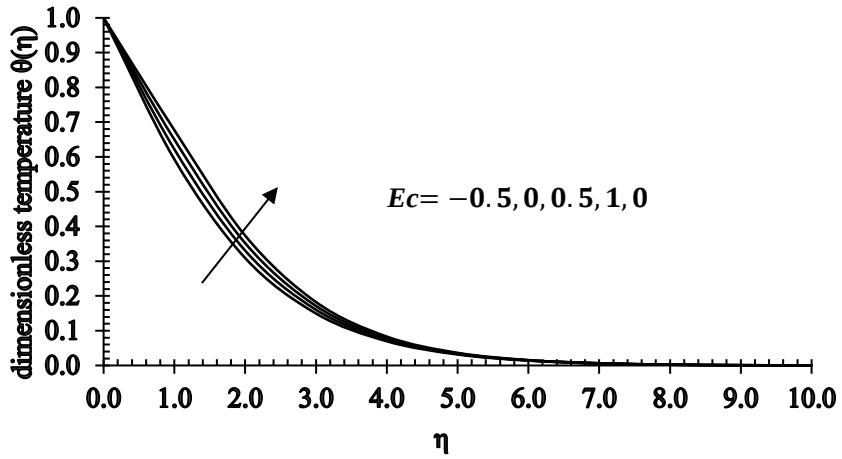


**Fig. 18.** Variation in temperature when $Ec$ is varied

*6.10 The impact of Chemical Reaction Parameter*

Figure 19 depicts the temperature distributions for various values of the chemical reaction parameter. The concentration of the fluid falls as the chemical reaction parameter increases.

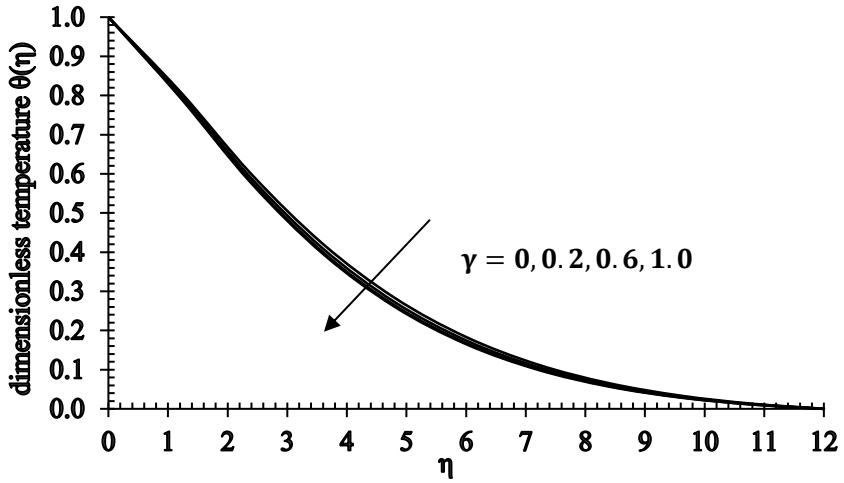


**Fig. 19.** Variation in temperature when $\gamma$ is varied

Figure 20 depicts the effect of the chemical reaction parameter on the concentration profile. It is observed that when the concentration of chemical reaction parameters increases, so does the thickness of the concentration. This is due to the fact that the chemical reaction in this system causes chemical dissipation, which causes a drop in the concentration profile. The chemical reaction has the greatest effect since it tends to reduce overshoot in concentration profiles and their related boundary layers.

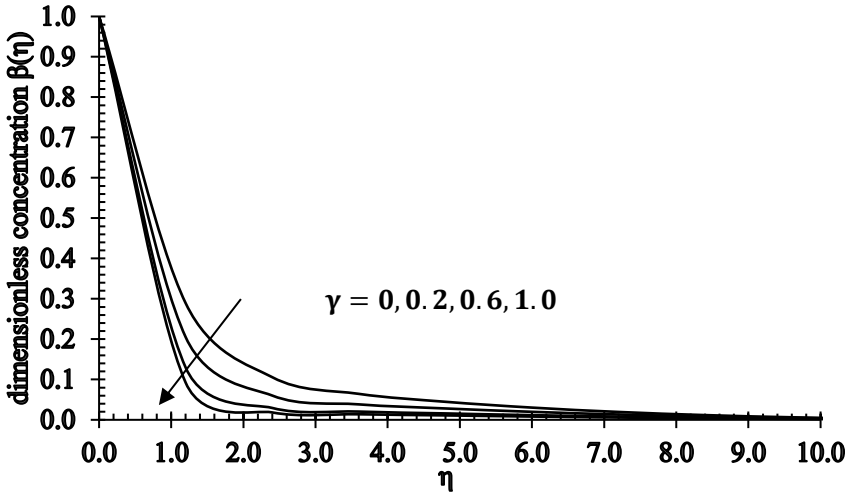


**Fig. 20.** Variation in concentration when $\gamma$ is varied

*6.11 Impact of Brownian Motion and Thermophoresis Parameter*

The influence of the Brownian motion parameter on concentration is seen in Figure 21. The concentration drops when the Brownian motion parameter is increased.

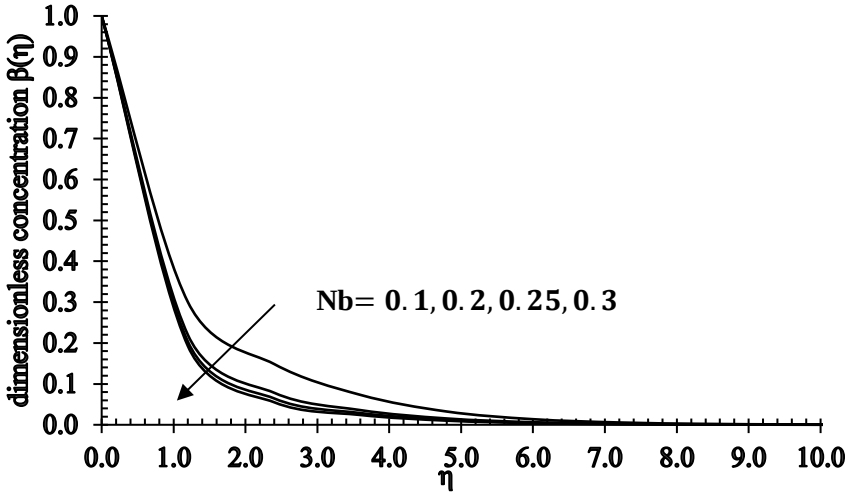


**Fig. 21.** Variation in concentration when $Nb$ is varied

Figure 22 depicts the influence of the thermophoresis parameter on the concentration of the flow field. Positive $Nt$ suggests a cool surface, whereas negative $Nt$ indicates a heated surface. As the thermophoresis parameter is increased, the concentration rises.

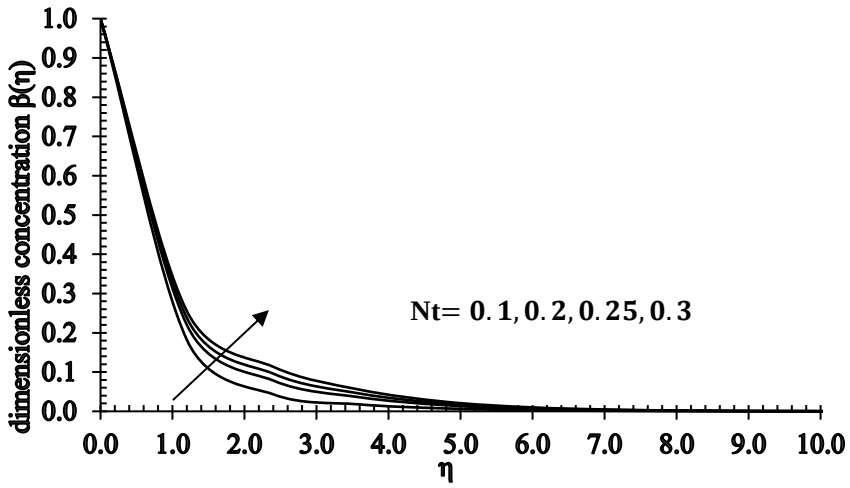


**Fig. 22.** Variation in concentration when $Nt$ is varied

## 7. Conclusions

We can draw the following conclusions from the preceding discussion:

i. Higher values of M lead to an elevation in the energy profile, while having the opposite effect on the velocity profile.
ii. An increase in the thermophoresis parameter results in an enhanced concentration profile.
iii. Mass transfer rate and heat transfer rate rise with an increase in thermal radiation.
iv. The velocity and temperature profiles are augmented by an increase in viscous dissipation.
v. The concentration field exhibits a decreasing trend for larger values of the Lewis number $(Le)$ and the chemical reaction parameter $(\chi)$.
vi. The velocity and temperature decrease as the Prandtl number $(Pr)$ increases.
vii. Temperature ascends with an increase in heat generation, stretching parameters, and solutal buoyancy force, while it decreases with an increase in the thermal buoyancy parameter and the Prandtl number.

## Acknowledgement
This research was not funded by any grant.

## References
[1] Crane, Lawrence J. "Flow past a stretching plate." *Zeitschrift für angewandte Mathematik und Physik ZAMP* 21 (1970): 645-647. https://doi.org/10.1007/BF01587695
[2] Mukhopadhyay, Swati. "Heat transfer analysis of the unsteady flow of a Maxwell fluid over a stretching surface in the presence of a heat source/sink." *Chinese Physics Letters* 29, no. 5 (2012): 054703. https://doi.org/10.1088/0256-307X/29/5/054703
[3] Sahoo, Bikash. "Effects of slip on sheet-driven flow and heat transfer of a non-Newtonian fluid past a stretching sheet." *Computers & Mathematics with Applications* 61, no. 5 (2011): 1442-1456. https://doi.org/10.1016/j.camwa.2011.01.017
[4] Rashidi, Mohammad Mehdi, Ali J. Chamkha, and Mohammad Keimanesh. "Application of multi-step differential transform method on flow of a second-grade fluid over a stretching or shrinking sheet." *American Journal of Computational Mathematics* 1, no. 02 (2011): 119-128. https://doi.org/10.4236/ajcm.2011.12012

[5] Ramzan, M., M. Farooq, A. Alsaedi, and T. Hayat. "MHD three-dimensional flow of couple stress fluid with Newtonian heating." *The European Physical Journal Plus* 128 (2013): 1-15. https://doi.org/10.1140/epjp/i2013-13049-5
[6] Makinde, O. D. "Analysis of Sakiadis flow of nanofluids with viscous dissipation and Newtonian heating." *Applied Mathematics and Mechanics* 33 (2012): 1545-1554. https://doi.org/10.1007/s10483-012-1642-8
[7] Ibrahim, F. S., A. M. Elaiw, and A. A. Bakr. "Influence of viscous dissipation and radiation on unsteady MHD mixed convection flow of micropolar fluids." *Appl. Math. Inf. Sci* 2 (2008): 143-162.
[8] Zhang, Chaoli, Liancun Zheng, Xinxin Zhang, and Goong Chen. "MHD flow and radiation heat transfer of nanofluids in porous media with variable surface heat flux and chemical reaction." *Applied Mathematical Modelling* 39, no. 1 (2015): 165-181. https://doi.org/10.1016/j.apm.2014.05.023
[9] Alam, M. S., M. M. Rahman, and M. A. Sattar. "On the effectiveness of viscous dissipation and Joule heating on steady Magnetohydrodynamic heat and mass transfer flow over an inclined radiate isothermal permeable surface in the presence of thermophoresis." *Communications in Nonlinear Science and Numerical Simulation* 14, no. 5 (2009): 2132-2143. https://doi.org/10.1016/j.cnsns.2008.06.008
[10] Hayat, T., Anum Naseem, M. Farooq, and A. Alsaedi. "Unsteady MHD three-dimensional flow with viscous dissipation and Joule heating." *The European Physical Journal Plus* 128 (2013): 1-15. https://doi.org/10.1140/epjp/i2013-13158-1
[11] Afify, Ahmed A. "MHD free convective flow and mass transfer over a stretching sheet with chemical reaction." *Heat and Mass Transfer* 40, no. 6-7 (2004): 495-500. https://doi.org/10.1007/s00231-003-0486-0
[12] Zhang, Chaoli, Liancun Zheng, Xinxin Zhang, and Goong Chen. "MHD flow and radiation heat transfer of nanofluids in porous media with variable surface heat flux and chemical reaction." *Applied Mathematical Modelling* 39, no. 1 (2015): 165-181. https://doi.org/10.1016/j.apm.2014.05.023
[13] Poornima, T., and N. Bhaskar Reddy. "Radiation effects on MHD free convective boundary layer flow of nanofluids over a nonlinear stretching sheet." *Advances in Applied Science Research* 4, no. 2 (2013): 190-202.
[14] Anwar, M. I., I. Khan, S. Sharidan, and M. Z. Salleh. "Conjugate effects of heat and mass transfer of nanofluids over a nonlinear stretching sheet." *International Journal of Physical Sciences* 7, no. 26 (2012): 4081-4092. https://doi.org/10.5897/IJPS12.358
[15] Rusdi, Nadia Diana Mohd, Siti Suzilliana Putri Mohamed Isa, Norihan Md Arifin, and Norfifah Bachok. "Thermal Radiation in Nanofluid Penetrable Flow Bounded with Partial Slip Condition." *CFD Letters* 13, no. 8 (2021): 32-44. https://doi.org/10.37934/cfdl.13.8.3244
[16] Bryant, Daniel John Ebrahim, and K. C. Ng. "Numerical Modelling of Hydraulic Jump Using Mesh-based CFD method and Its Comparison with Lagrangian Moving-Grid Approach." *Journal of Advanced Research in Micro and Nano Engineering* 10, no. 1 (2022): 1-6.
[17] Ramanuja, Mani, J. Kavitha, A. Sudhakar, A. Ajay Babu, Hari Kamala Sree, and K. Ramesh Babu. "Effect of Chemically Reactive Nanofluid Flowing Across Horizontal Cylinder: Numerical Solution." *Journal of Advanced Research in Numerical Heat Transfer* 12, no. 1 (2023): 1-17.
[18] Mahat, Rahimah, Sharidan Shafie, and Imran Ullah. "Free Convection of Viscoelastic Nanofluid Flow on a Horizontal Circular Cylinder with Constant Heat Flux." *Journal of Advanced Research in Applied Sciences and Engineering Technology* 30, no. 3 (2023): 1-8. https://doi.org/10.37934/araset.30.3.18
[19] Priyanka, Patil, Shaimaa AM Abdelmohsen, Jagadish V. Tawade, Abdelbacki MM Ashraf, Raman Kumar, and Mahadev M. Biradar. "Multiple slip effects of MHD boundary-layer motion of a Casson nanoliquid over a penetrable linearly stretching sheet embedded in non-Darcian porous medium." *International Journal of Modern Physics B* 37, no. 03 (2023): 2350022. https://doi.org/10.1142/S0217979223500224
[20] Tawade, Jagadish V., C. N. Guled, Samad Noeiaghdam, Unai Fernandez-Gamiz, Vediyappan Govindan, and Sundarappan Balamuralitharan. "Effects of thermophoresis and Brownian motion for thermal and chemically reacting Casson nanofluid flow over a linearly stretching sheet." *Results in Engineering* 15 (2022): 100448. https://doi.org/10.1016/j.rineng.2022.100448
[21] Guled, C. N., J. V. Tawade, Mahantesh M. Nandeppanavar, and A. R. Saraf. "MHD slip flow and heat transfer of UCM fluid with the effect of suction/injection due to stretching sheet: OHAM solution." *Heat Transfer* 51, no. 4 (2022): 3201-3218. https://doi.org/10.1002/htj.22444
[22] Abel, M. Subhas, Jagadish Tawade, and Mahantesh M. Nandeppanavar. "Effect of non-uniform heat source on MHD heat transfer in a liquid film over an unsteady stretching sheet." *International Journal of Non-Linear Mechanics* 44, no. 9 (2009): 990-998. https://doi.org/10.1016/j.ijnonlinmec.2009.07.004
[23] Subhas Abel, M., Jagadish V. Tawade, and Mahantesh M. Nandeppanavar. "MHD flow and heat transfer for the upper-convected Maxwell fluid over a stretching sheet." *Meccanica* 47 (2012): 385-393. https://doi.org/10.1007/s11012-011-9448-7

[24] Sarfraz, Mahnoor, Masood Khan, and Muhammad Yasir. "Dynamics of water conveying iron oxide and graphene nanoparticles subject to stretching/spiraling surface: An asymptotic approach." *Ain Shams Engineering Journal* 14, no. 8 (2023): 102021. https://doi.org/10.1016/j.asej.2022.102021

[25] Khan, Masood, Mahnoor Sarfraz, Jawad Ahmed, Latif Ahmad, and Awais Ahmed. "Viscoelastic nanofluid motion for Homann stagnation-region with thermal radiation characteristics." *Proceedings of the Institution of Mechanical Engineers, Part C: Journal of Mechanical Engineering Science* 235, no. 21 (2021): 5324-5336. https://doi.org/10.1177/0954406220987266

[26] Khan, M., J. Ahmed, F. Sultana, and M. Sarfraz. "Non-axisymmetric Homann MHD stagnation point flow of Al 2 O 3-Cu/water hybrid nanofluid with shape factor impact." *Applied Mathematics and Mechanics* 41 (2020): 1125-1138. https://doi.org/10.1007/s10483-020-2638-6

[27] Sarfraz, Mahnoor, and Masood Khan. "Significance of ethylene glycol-based CNT Homann nanofluid flow over a biaxially stretching surface." *Waves in Random and Complex Media* (2022): 1-15. https://doi.org/10.1080/17455030.2022.2075048

[28] Narender, Ganji, Kamatam Govardhan, and Gobburu Sreedhar Sarma. "Magnetohydrodynamic stagnation point on a Casson nanofluid flow over a radially stretching sheet." *Beilstein Journal of Nanotechnology* 11, no. 1 (2020): 1303-1315. https://doi.org/10.3762/bjnano.11.114

[29] Narender, G., K. Govardhan, and G. Sreedhar Sarma. "Viscous dissipation and thermal radiation effects on the flow of Maxwell nanofluid over a stretching surface." *International Journal of Nonlinear Analysis and Applications* 12, no. 2 (2021): 1267-1287.

[30] Narender, G., K. Govardhan, and G. Sreedhar Sarma. "MHD Casson nanofluid past a stretching sheet with the effects of viscous dissipation, chemical reaction and heat source/sink." *Journal of Applied and Computational Mechanics* (2019).

[31] Makinde, Oluwole Daniel, Fazle Mabood, and Mohammed S. Ibrahim. "Chemically reacting on MHD boundary-layer flow of nanofluids over a non-linear stretching sheet with heat source/sink and thermal radiation." (2018). https://doi.org/10.2298/TSCI151003284M